Nonlinear evolution of unstable fluid interface

S. I. Abarzhi*

Department of Applied Mathematics and Statistics, State University of New York at Stony Brook, Stony Brook, New York 11794-3600

(Received 8 June 2001; revised manuscript received 11 April 2002; published 11 September 2002)

We study the coherent motion of bubbles and spikes in the Richtmyer-Meshkov instability for isotropic three-dimensional and two-dimensional periodic flows. For equations governing the local dynamics of the bubble, we find a family of regular asymptotic solutions parametrized by the principal curvature at the bubble top. The physically significant solution in this family corresponds to a bubble with a flattened surface, not to a bubble with a finite curvature. The evolution of the bubble front is described and the diagnostic parameters are suggested.

DOI: 10.1103/PhysRevE.66.036301 PACS number(s): 47.20.Bp, 47.20.Ma, 47.20.Ky, 52.35.Py

I. INTRODUCTION

When a light fluid accelerates a heavy fluid, the misalignment of the pressure and density gradients gives rise the instability of the interface, and produces eventually the turbulent mixing of the fluids [1]. This phenomenon is called the Rayleigh-Taylor instability (RTI), if the acceleration is sustained, and the Richtmyer-Meshkov instability (RMI), if the acceleration is driven by shock or impulsive [2,3]. The RT-RM turbulent mixing controls many physical and technological processes such as supernova explosion, inertial confinement fusion, flames, etc. [1]. Reliable description of the turbulent mixing is the basic objective of studies of the RT-RM instabilities [4–10]. The cascades of energy, the dynamics of small-scale structures, and the dynamics of the large-scale coherent structure are the fundamental issues to be understood.

The large-scale coherent structure occurs in the nonlinear regime of RTI and RMI. It is a periodic array of bubbles and spikes in the plane normal to the direction of gravity or the initial shock [1,4,6]. The light fluid penetrates the heavy fluid in bubbles, and the heavy fluid penetrates the light fluid in spikes [1–3]. The secondary instabilities and vorticity [10] result in singularities. Therefore the nonlinear evolution of the unstable fluid interface is very complicated [1–3]. Starting from the works of Layzer [11] and Garabedian [12] in 1950s, various methods have been developed to study the singularities and the interplay of harmonics in two-dimensional (2D) Rayleigh-Taylor flows [11–19]. For three-dimensional RTI a new approach based on group theory has been proposed recently in Refs. [18,19]. The asymptotic 2D and 3D theories agreed with experiments and simulations. For the Richtmyer-Meshkov instability, theories [20–22] explained experimental [1,3] and numerical data [23–28] in the linear regime; the nonlinear dynamics of RMI is not understood well.

Here we study the large-scale coherent motion in the Richtmyer-Meshkov instability and report the theoretical solutions, which capture the interplay of harmonics in the nonlinear dynamics of isotropic three- and two-dimensional periodic flows. The evolution of the bubble front is described. It is shown that asymptotically the RM bubbles flatten with time and the shapes of the Rayleigh-Taylor and Richtmyer-Meshkov bubbles differ significantly. The theory explains existing data qualitatively and establishes the diagnostic parameters for experiments.

The paper is organized as follows. In Sec. II the problem is formulated, and previous approaches and results are reviewed. In Sec. III we derive a dynamical system of ordinary differential equations governed by the local dynamics of the nonlinear bubble. In Sec. IV a family of regular asymptotic solutions to the system is found, and the physically significant solution in the family is chosen. In Sec. V we discuss the local dynamics of the RM bubbles and compare it with existing data and with the RT case.

II. THE PROBLEM FORMULATION

In the nonlinear regime of RMI, the interface evolves with no external forces, the growth rates of bubbles and spikes decreases with time [1,3], and the fluid motion becomes incompressible [7–10]. Based on the experimental observations [8–10,24–28], we generalized the idea suggested in Ref. [29] and divide the fluid interface into active and passive regions. In the active regions (small scales) the vorticity is intensive, while the passive regions (large scales) are simply advected. A significant part of the fluid energy is concentrated in the large-scale coherent motion. To describe the dynamics of the coherent structure, one can apply the spectral approach and group theory, and the potential approximation. For fluids with highly contrasting densities (fluid-vacuum), the governing equations have the form

$$\Delta\Phi=0, \quad \frac{\partial\Phi}{\partial t}+\frac{1}{2}(\nabla\Phi)^2\big|_{\theta=0}=0,$$

$$\frac{\partial\theta}{\partial t}+\nabla\theta\cdot\nabla\Phi\big|_{\theta=0}=0, \quad \nabla\Phi\big|_{z=+\infty}=\mathbf{0}. \tag{1}$$

Here $\Phi(x,y,z,t)$ is the fluid potential, $\theta(x,y,z,t)=z^*(x,y,t)-z$ is the scalar function, $z^*(x,y,t)$ is the fluid-free surface, assuming the fluid is located in the region $\theta<0$, (x, y, z) are the Cartesian coordinates, and t is time. The

*Email address: snezha@ams.sunysb.edu; present address: Center for Turbulence Research, Stanford University, Bldg. 500, 488 Escondido Mall, Stanford, CA 94305-3030.

first of the boundary conditions at the free surface in Eq. (1) is derived from the equation for momentum conservation, and the second one is derived from the equation of continuity. Initially, $t=t_0$, both geometry $z^*(x,y,t_0)$ and velocity $\boldsymbol{\nu}^{(0)}=\boldsymbol{\nabla}\Phi(x,y,z,t_0)|_{z=z^*}$ of the free surface are slightly perturbed. The initial conditions determine the length scale (i.e., spatial period) λ, the time scale $\tau\sim\lambda/|\nu^{(0)}|$, and symmetry of the flow in Eq. (1) [29]. We choose the value of the period in the vicinity of the wavelength $\lambda_{\max}$, which corresponds to the mode of fastest growth established in real fluids by surface tension and viscosity [30]. As a group of symmetry of the flow in Eq. (1), we choose a spatial symmorphic group with translations in the plane (x, y) and with inversion $x\rightarrow -x$ and $y\rightarrow -y$, such as hexagonal, square, rectangular, rhombic, or oblique [31]. The coherent structure of bubbles and spikes must be invariant under one of these groups in order to be stable under large-scale modulations [18,19].

To date, no exact analytical solution to the problem (1) has been found. Several authors [1,29,32–35] have studied the flow in Eq. (1) using the so-called Layzer-type approach [11]. Under this approach, the fluid potential is represented by a single Fourier harmonics. The nonlinear equations in Eq. (1) are then reexpanded in the lowest order near the top of the bubble or spike and reduced to a system of ordinary differential equations [11,29,32–35]. In two dimensions, Shvarts [32] has found an asymptotic solution for the system describing the nonlinear RM bubble. Inogamov [33] has integrated the ODEs and concluded that this regular solution is a stable node. Mikaelian [34] and Zhang [35] have integrated the ODEs for a special class of initial conditions and derived the same regular asymptotic solution. Zhang [35] has suggested to describe the motion of the spike by a singular asymptotic solution for the equations. In Ref. [29], the ODEs have been integrated in both 3D and 2D cases for a wide class of initial conditions, and the stability analysis has been performed. It has been shown that the field of the initial velocity determines regular or singular behavior of late-time asymptotes [29]. The singular spike dynamics is governed by the initial conditions, in agreement with Ref. [35]. The velocity of the regular bubble decreases asymptotically with time, and its curvature approaches a finite value independent of the initial conditions [29]. This regular Layzer-type solution is not a stable node, as was predicted in Ref. [33].

Reflecting some important features of RMI dynamics, the Layzer-type approach has, however, a number of limitations. The most serious disadvantage is that the method does not capture the interplay of harmonics in the nonlinear regime and fails when the number of harmonics exceeds one [29]. The properties of the Layzer-type bubble in RMI also raise some doubts. In single-mode approximation, the curvature of the nonlinear bubble is the same in the case of sustained (RTI) or impulsive (RMI) acceleration [29]. This equality of shapes follows from a specific degeneracy of Layzer-type ODEs [29], and cannot be a universal nonlinear property. The RT flow is driven by buoyancy, while RMI is inertial instability. Since the nonlinear RM bubbles decelerate, they may not be curved. Remarkably, in many experiments and simulations on RMI a tendency of the bubbles to be flattened at the top has been observed, but has never been discussed [8–10,24–28]. Below we show that a multiple harmonic analysis resolves all these issues.

III. DYNAMICAL SYSTEM

To find the nonlinear solution, we reduce the equations in Eq. (1) to a dynamical system governing the local dynamics of the bubble as in Refs. [18,19]. To simplify the calculations, we switch to the frame of references moving with velocity $\nu(t)$ in the z direction, where $\nu(t)$ is the velocity at the bubble top in the laboratory frame of references. In the moving frame of references, fluid influences an effective acceleration. In Eq. (1), the term $z\partial\nu/\partial t|_{z=z}$ must be added on the left-hand side of the momentum equation, the continuity equation remains unchanged, and the boundary condition at $z=+\infty$ is $(\partial\Phi/\partial z)|_{z=+\infty}=-\nu$.

For a 3D flow with square symmetry in the plane (x, y), the fluid potential is represented by a Fourier series

$$\Phi=\sum_{m,n=0}^{\infty}\Phi_{mn}(t)[\cos(mkx)\cos(nky)\times\exp(-kz\alpha_{mn})/k\alpha_{mn}+z],$$

where $k=2\pi/\lambda$ is the wave vector, λ is the spatial period, $\alpha_{mn}=\sqrt{m^2+n^2}$, m and n are integers, $\Phi_{mn}=\Phi_{nm}$ due to symmetry, and $\Phi_{00}=0$. The bubble top with coordinates (0,0,0) is the point of stagnation. The boundary condition at $z=+\infty$ gives $\Sigma_{m,n=0}^{\infty}\Phi_{mn}=-\nu$. For $x\approx 0$, $y\approx 0$ the free surface can be expanded as a power series, $z^*\mp\Sigma_{i,j=0}^{\infty}\zeta_{ij}(t)x^{2i}y^{2j}$, with $\zeta_{ij}=\zeta_{ji}$ and $\zeta_{00}=0$. Substituting these expressions in z components in the nonlinear equations in Eq. (1) we reexpand Eq. (1) for $x\approx 0$, $y\approx 0$ as a power series in terms of $x^{2i}y^{2j}$, where $i+j=N=1,2,...,\infty$ is the order of approximation. In this way we derive a dynamical system of ordinary differential equations in terms of surface variables ζ_{ij} and moments $M_{a,b,c}(t)=\Sigma_{m,n=0}^{\infty}\Phi_{mn}(t)k^{a+b+c}m^a n^b\alpha_{mn}^c$ with integer a, b, and c,

$$N=1,\quad -\dot{M}_0\zeta_1-\dot{M}_1/2+M_1^2/2=0,\quad \dot{\zeta}_1-4\zeta_1M_1-M_2/2=0, \tag{2}$$

$$N=2,\quad -\dot{M}_0\zeta_{20}+\dot{M}_2\zeta_1/2+\dot{M}_1\zeta_1^2+\dot{M}_3/4!+3M_2^2/8-M_1M_3/6+3M_1M_2\zeta_1+10M_1^2\zeta_1^2=0,$$

$$-\dot{M}_0\zeta_{11}+\dot{M}_2\zeta_1+2\dot{M}_1\zeta_1^2+\dot{M}_{2,2,-1}/4+3M_2^2/4-M_1M_{2,2,-1}+6M_1M_2\zeta_1+20M_1^2\zeta_1^2=0,$$

$$\dot{\zeta}_{20}-6\zeta_{20}M_1+\zeta_1(5M_3+3M_{2,2,-1})/6+3M_2\zeta_1^2+M_4/4!=0,$$

$$\dot{\zeta}_{11}-6\zeta_{11}M_1+\zeta_1(M_3+3M_{2,2,-1})+6M_2\zeta_1^2+M_{220}/4=0.$$

In Eq. (2) dot indicates time derivative, $\zeta_1=\zeta_{10}$ is the principal curvature at the bubble top, and the other notations are $M_1=M_{2,0,-1}$, $M_2=M_{2,0,0}$, $M_3=M_{4,0,-1}$, $M_4=M_{4,0,0}$, and $M_0=M_{0,0,0}=-\nu$ (see Appendix).

The equations in [Eq. (2), Appendix] govern the local dynamics of the bubble as long as the cascade of energy is insignificant and the spatial period λ of the coherent structure is invariable. Moments $M_{a,b,c}$ are correlation functions by physical meaning. They involve infinite series of harmonics. This presentation allows one to perform a multiple harmonic analysis. The local dynamical system (2) cannot be integrated explicitly. At every N in Eq. (2) (see Appendix) the number of moments $M_{a,b,c}$ and surface variables ζ_{ij} is larger than the number of equations. A truncation is required to find an approximate asymptotic solution. For physical solutions to the local system, the Fourier amplitudes decay with increase in their number and the approximations converge.

To find a time dependence of the regular asymptotic solutions in Eq. (2) (see Appendix) in main order as $t/\tau \to \infty$, we substitute $M \sim t^a$ and $\zeta \sim t^b$ into the ODEs and obtain $a-1=b=0$. Therefore for the nonlinear bubbles the surface variables ζ_{mn} become asymptotically time independent, while the moments $M_{a,b,c}$, the amplitudes Φ_{mn}, and velocity ν decay as $1/t$ [29,32–35]. With this time dependence, the equations in Eq. (2) (see Appendix) become algebraic and seem to be easily resolved. However, the interplay of harmonics in the nonlinear problem (1) and, consequently, the manner of truncation in the local system (2) are nontrivial issues [29].

IV. REGULAR ASYMPTOTIC SOLUTIONS

Retaining only the first-order harmonics in the expressions for the moments, $\Phi_{10}=M_1/k=M_2/k^2=M_0/2$, one derives at $N=1$ in Eq. (2) the nonlinear asymptotic solution of the Layzer type [11,29]. The velocity of the Layzer-type bubble in Eq. (2) is $\nu=1/kt$ and the curvature $\zeta_1=-k/8$ [29]. In second and higher orders of approximation the equations for coefficients in the Layzer-type expansion have no real solutions. This reveals deficiency of the method. There is no Layzer-type asymptotic solution, only a Layzer-type first-order approximation. A similar conclusion has been drawn in Refs. [18], [19] in the case of RT bubbles.

To find a multiple harmonic description of the bubble motion, we apply the following idea. For the flow in Eq. (1), the nonlinearity is nonlocal. Singularities determine the interplay of harmonics in the local system and, therefore, the shape of the regular bubble. Assuming the bubble shape is free and is parametrized by the principal curvature(s) at the top, we find a continuous family of regular asymptotic solutions for Eqs. (1) and (2). For solutions in this family, the interplay of harmonics is well captured. The family involves all bubbles allowed by symmetry of the global flow. The symmetry determines the number of the family parameters. We choose the fastest stable solution in the family as the physically significant one.

To construct the family of asymptotic solutions, we use the manner of truncation as in Refs. [18,19]. At a given N in Eq. (2) (see Appendix), let N_e be the number of equations and N_t be the number of variables (the surface variables and the Fourier amplitudes or independent moments taken for truncation). The difference $N_p=N_t-N_e$ determines the number of free parameters in Nth approximation. At $N_p=0$ the solution for the system is a point; at $N_p=1$ solutions form a one-parameter curve, at $N_p=2$ solutions form a two-parameter surface, etc. The number of parameters N_p in the complete system (2) (see Appendix) must be such that at every N the asymptotic solutions exist, and as N increases, they converge. Both criteria are satisfied only if the number of parameters N_p in the local system is that number required by symmetry of the global flow. By physical meaning, these free parameters are the principal curvatures at the bubble top and their position with respect to the axes, so $N_p \leqslant 3$ [31,36]. For 3D bubbles with square symmetry as well as for 3D hexagonal or 2D bubbles the number of free parameters in Eq. (2) is $N_p=1$ [18,19,36].

At every N in Eq. (2) (see Appendix) we take $N_t=N_e+1$ and establish additional relations between the moments. Then, impressing conditions $\zeta_{mn}(t)=\zeta_{mn}$, $\Phi_{mn}(t)=\varphi_{mn}/t$, and $M_{a,b,c}(t)=m_{a,b,c}/t$ [or $M_n(t)=m_n/t$], and keeping the curvature value ζ_1 free, we find the velocity, the amplitudes, and the surface variables as functions on this parameter, i.e., one-parameter family of regular asymptotic solutions. For every N, $\zeta_1=-m_2/8m_1$ and $2\zeta_1 m_0=-m_1(1+m_1)$. In the first approximation in Eq. (2), $N=1$, $N_e=2$ and $N_t=3$, and with the amplitudes Φ_{10}, Φ_{20} retained in the expressions for the moments $m_0=2(\varphi_{10}+\varphi_{20})=3m_1/k-m_2/k^2$ and $m_1=-(2\zeta_1/k)[3+8(\zeta_1/k)]-1$; the family of solutions has the form

$$\zeta_1=-1/2R, \quad \nu=(3kR-4)[(kR)^2-3kR+4]/(kR)^3kt, \tag{3}$$

$$\Phi_{10}=-2(kR-2)[(kR)^2-3kR+4]/(kR)^3kt,$$

$$\Phi_{20}=(kR-4)[(kR)^2-3kR+4]/2(kR)^3kt.$$

In the second approximation in Eq. (2), $N=2$, $N_e=6$ and $N_t=7$, four harmonics are retained, Φ_{10}, Φ_{11}, Φ_{20}, and Φ_{30}, and variable m_1 obeys a fourth-order equation with coefficients dependent on ζ_1. Analogously, regular asymptotic solutions could be found in higher approximations. Figures 1 and 2 show the analytical results. We describe the family properties.

In the physical region $kR_{\rm cr} \leqslant kR \leqslant \infty$, the velocity is $\nu=l(kR)/(kt)$, the Fourier amplitudes decay with increase in their number, the lowest-order amplitude is dominant, and the approximations converge, Figs. 1, 2(a)–2(b). The function $l(kR)$ is a function on the radius of curvature, similar to Eq. (3). Over a wide interval of kR, $l(kR)$ is insensitive to higher-order terms, Figs. 1 and 2(b). The critical solution $R_{\rm cr} \sim 3/k$ with $\nu_{\rm cr} \sim 0.74/(kt)$ bounds the physical region: the bubble cannot be very curved. At $R \sim R_{\rm cr}$ the amplitudes $|\Phi_{(m+1)n}| \sim |\Phi_{mn}|$, and for $R<R_{\rm cr}$ the approximations diverge, Fig. 2. The Layzer-type solution can be derived from the condition $\Phi_{20}=0$ in Eq. (3). Remarkably, higher-order corrections for the velocity of this solution are less than 1%, Figs. 1 and 2(b). The bubble velocity is an increasing function on the radius of curvature, and as $kR \to \infty$ the velocity approaches its maximum value ν_∞, Fig. 1. For a flattened bubble in Nth approximation, the curvature $(\zeta_1/k) \sim 0$ and $(m_1+1) \sim (\zeta_1/k)$, so $\lim_{(\zeta_1/k)\to 0}(m_1+1)/(\zeta_1/k)$ is deter-

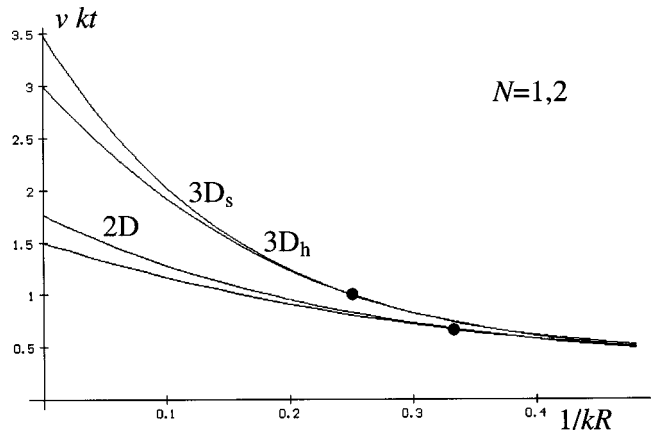

FIG. 1. Family of regular asymptotic solutions in RMI. Velocity ν as the function on the radius of curvature R; k is the wave vector, t is time, N is order of approximation. Three-dimensional flows with square ($3D_s$) and hexagonal ($3D_h$) symmetry and two-dimensional (2D) flow. Black circles mark the Layzer-type solutions with $R=4/k$ in 3D, and $R=3/k$ in 2D.

mined, and the velocity is $[\nu_\infty]_N=-m_1(1+m_1)/2\zeta_1 t \approx C_N/kt$, where C_N is a constant. First few approximations do not give very precise value of ν_∞, which is more sensitive to terms neglected in the truncation than the velocity of a bubble with a finite curvature. However, the higher-order corrections for ν_∞ are reasonably small, $[\nu_\infty]_{N=2}/[\nu_\infty]_{N=1} \approx 1+e^{-2}$, Fig. 2(b), and up to third-order harmonics, the solution with $kR\equiv\infty$ remains smooth and does not blow up, Fig. 2(a). We roughly estimate the velocity of the flattened bubble as $\nu_\infty \sim 4/kt$. In higher approximations the value of ν_∞ can be determined more accurately.

To analyze stability of the family solutions we slightly perturb $\zeta_{mn}\to\zeta_{mn}+\theta_{mn}(t)$, and $M_{a,b,c}\to[m_{a,b,c}+\Delta_{a,b,c}(t)]/t$. Substituting these expressions in Eq. (2) and expanding them for small Δ and θ, we find $\Delta_{a,b,c}(t) \sim A_{a,b,c}t^\alpha$ and $\theta_{mn}(t)\sim B_{mn}t^\beta$, where $A_{a,b,c}$ and B_{mn} are some constants, and the exponents $\alpha=\beta$ are the functions on the radius of curvature, $\beta=\beta(kR)$. Therefore, asymptotically the velocity $|\nu(t)-l(kR)/(kt)|\sim t^{\beta-1}$ and the curvature $|\zeta_1(t)+1/(2R)|\sim t^\beta$. For stable solutions the real part of exponents β must be negative, $\mathrm{Re}[\beta]<0$.

At every N in Eq. (2) with $\Delta_{a,b,c}(t)\sim A_{a,b,c}t^\beta$ and $\theta_{mn}(t)\sim B_{mn}t^\beta$, we keep the highest order amplitude unperturbed and establish additional relations between the $\Delta_{a,b,c}$ so that the number of independent Δ and θ (or A's and B's) equals N_e. The exponents $\beta(kR)$ are then defined by the condition that the determinant of the linear algebraic system for independent A's and B's equals zero. At $N=1$, $\Delta_0=\Delta_1/k=\Delta_2/k^2$, the exponent β obeys quadratic equation with coefficients depending on the curvature, and $\mathrm{Re}[\beta]<0$ for $kR>2$. At $N=2$, the exponent β obeys a sixth-order equation, and $\mathrm{Re}[\beta]<0$ for $kR>3.6$, etc. As is seen from Fig. 3, solutions with $R\sim R_{\mathrm{cr}}$ are unstable. As N increases and higher-order terms are involved, solutions with $R\sim\lambda/2$ lose stability while solutions with $kR\to\infty$ remain stable. For $kR\equiv 0$ the highest exponent is $\mathrm{Re}[\beta_\infty]=-2.42$ $(N=2)$, so this bubble flattens in time as $kR\sim(t/\tau)^{|\mathrm{Re}[\beta_\infty]|}$. The real value of

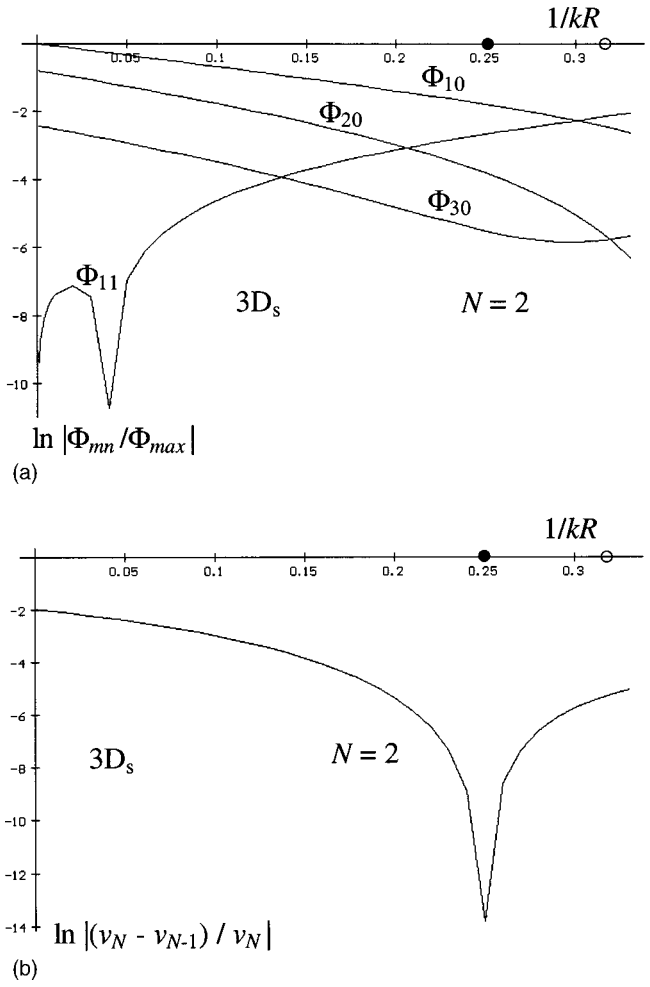

FIG. 2. Family of regular asymptotic solutions in RMI. (a) Exponential decay of the absolute value of the Fourier amplitudes Φ_{mn}. (b) Exponential decay of the absolute value of $(\nu_N-\nu_{N-1})/\nu_N$. Three-dimensional flow with square symmetry, $3D_s$; N is the order of approximation; R is the radius of curvature; k is the wave vector; $\Phi_{\max}=\Phi_{10}(kR\equiv\infty)$. The black circle marks the Layzer-type solution, and the white circle marks the critical solution $R\sim R_{\mathrm{cr}}$.

β_∞ depends weakly on higher order amplitudes, Fig. 3 (at $N=1$, $\mathrm{Re}[\beta_\infty]=-5/2$). This suggests that the flattening process is dominated by the lowest-order terms.

To conclude this section for equations governing the local dynamics of the RM bubble, we found a continuous family of regular asymptotic solutions parametrized by the principal curvature at the bubble top, and studied the stability of the solutions. The nonlinear solutions are multiple harmonic solutions. Our analysis can be extended to higher approximations. Over the family, the interplay of harmonics is well captured, and the lowest-order Fourier amplitude is dominant. For bubbles with a finite curvature, the velocity is insensitive to terms neglected in the truncation. These solutions, however, lose stability when higher-order terms are involved. For a flattened bubble, the velocity is sensitive to terms neglected in the truncation, but the higher-order corrections are small. This solution is stable, and the flattening exponent depends weakly on terms of the higher order. The fastest stable solution in the asymptotic family corresponds

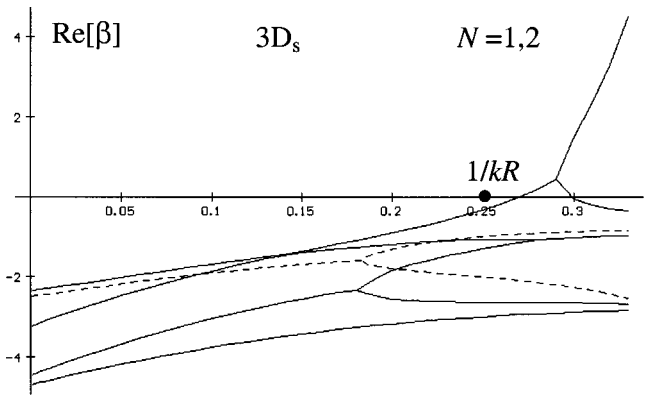

FIG. 3. Stability analysis for the family of regular asymptotic solutions in RMI. Real part of exponents β as the function on the radius of curvature R. Three-dimensional flow with square symmetry, $3D_s$. Dashed lines correspond to $N=1$, solid lines correspond to $N=2$, the black circle marks the Layzer-type solution $R_L=4/k$.

to a bubble with a flattened surface, not to a bubble with a finite curvature.

A. Regular asymptotic solutions for 3D flow with hexagonal symmetry

The obtained results are generalized directly for a 3D flow with a hexagonal group of invariance. For highly symmetric 3D flows (square, hexagonal) the asymptotic solutions and their stability behavior coincide except for the difference in the normalization factor k, Fig. 1 [37]. The physical reason of this universality is a near-circular contour of the bubble [18,19]. To explain this statement, we make the expansion of the free surface [as well the equations in Eq. (1)] in the form $z^*=\Sigma_{m=1}^{\infty}\xi_m(x^2+y^2)^m+$(other terms of the form $\vartheta_{ij}x^{2i}y^{2j}$, which break the circularity). For square symmetry these noncircular terms appear at $i+j=2m$, m is an integer, for example, x^2y^2, $(x^2y^4+x^4y^2)$; in the case of hexagonal symmetry they appear at $i+j=3m$, for example, $(x^2y^4+x^4y^2)$. The solutions for square and hexagonal systems may have a universal form only if the contribution of the noncircular terms to the dynamics is negligibly small.

The highly symmetric 3D bubbles in RMI have a near-circular contour and a universal dynamics in the units of the wave vector k, Fig. 1 [37]. For 3D flow with hexagonal symmetry $k=4\pi/\sqrt{3}\lambda$, and at a fixed value of period λ and at the same value of the parameter kR, 3D hexagonal bubbles are slower and narrower than 3D square ones. For a hexagonal bubble with $kR\equiv\infty$ the highest exponent is $\mathrm{Re}[\beta_\infty]=-2.44$ at $N=2$.

B. Regular asymptotic solutions for 2D flow

For a 2D flow, the potential is

$$\Phi(x,z,t)=\Sigma_{m=1}^{\infty}\Phi_m(t)[\exp(-mkz)\cos(mkx)/mk+z],$$
$$k=2\pi/\lambda.$$

Near the top of the bubble the free surface is $z^*(x,t)=\Sigma_{m=1}^{\infty}\zeta_m(t)x^{2m}$, and with moments $M_n(t)=\Sigma_{m=1}^{\infty}\Phi_m(t)(km)^n$, one derives from Eq. (1)

TABLE I. Comparison of parameters of the Layzer-type bubble (velocity ν_L and curvature radius R_L), with the flattened bubble [velocity ν_∞ and curvature radius $R\sim(t/\tau)^{\mathrm{Re}[\beta_\infty]}/k$] for 3D flows with square, $3D_s$, and hexagonal, $3D_h$, symmetry as well as 2D flow in units of wave vector k and spatial period λ.

	$\nu_L kt$	kR_L	$\nu_\infty kt$	$\mathrm{Re}[\beta_\infty]$
$3D_s$	1	4	4	−2.42
$3D_h$	1	4	4	−2.44
2D	2/3	3	2	−2.27
	$\frac{\nu_L t}{(\lambda/2)}$	$\frac{R_L}{(\lambda/2)}$	$\frac{\nu_\infty t}{(\lambda/2)}$	$\mathrm{Re}[\beta_\infty]$
$3D_s$	0.32	1.27	1.28	−2.42
$3D_h$	0.28	1.10	1.12	−2.24
2D	0.22	0.96	0.66	−2.27

$$N=1,\quad -\dot{M}_0\zeta_1-\dot{M}_1/2+M_1^2/2,=0,\quad \dot{\zeta}_1-3\zeta_1M_1-M_2/2=0, \tag{4}$$

$$N=2,\quad \dot{\zeta}_2-5\zeta_2M_1+5\zeta_1M_3/6+5\zeta_1^2M_2/2+M_4/4!=0,$$
$$-\dot{M}_0\zeta_2+\dot{M}_2\zeta_1/2+\dot{M}_1\zeta_1^2/2+\dot{M}_3/4!$$
$$+3M_2^2/8-M_1M_3/6+3M_1M_2\zeta_1/2+7M_1^2\zeta_1^2/2=0.$$

The 2D and 3D results are similar, and Table I gives some quantitative values. In the first approximation, $N=1$, the 2D family of regular asymptotic solutions takes the form

$$\zeta_1=-1/2R,\quad \nu=3(Rk-1)[2(Rk)^2-3Rk+3]/4(Rk)^3kt, \tag{5}$$

$$\Phi_1=-(2kR-3)[2(kR)^2-3kR+3]/2(kR)^3kt,$$

$$\Phi_2=(kR-3)[2(kR)^2-3kR+3]/4(kR)^3kt.$$

In 2D family the critical solution is $R_{cr}\sim 2/k$ and $\nu_{cr}\sim 0.47/(kt)$, and for $kR_{cr}\leqslant kR\leqslant\infty$ the approximations converge. The Layzer-type solution has $R_L=3/k\sim 0.96(\lambda/2)$ and $\nu_L=2/3kt$ [29,32–35]. As N increases, solutions with $R\sim\lambda/2$ lose stability. For a flattened 2D bubble, $kR\equiv\infty$, the velocity is estimated as $\nu_\infty\sim 2/kt$. This solution is stable and the highest exponent $\mathrm{Re}[\beta_\infty]=-2.27$ at $N=2$.

V. DISCUSSION

We have performed a multiple harmonic analysis of the coherent motion in the Richtmyer-Meshkov instability. Our approach to the problem is an extent of the method developed in Refs. [18,19] for the RT flow, and it is based on group theory. For a periodic array of bubbles and spikes in RMI, we determined symmetry groups, providing stability of the coherent structure under large-scale modulations [18,19]. Then, using the Fourier expansion and the spatial Taylor expansion, we derived from the conservation laws a dynamical system of ODEs governing the local dynamics of the bubble. Due to singularities, the interplay of harmonics in the local system is a nontrivial issue [29]. To capture the interplay of

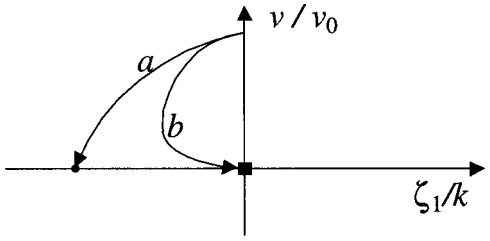

FIG. 4. Schematic plot of the dynamics trajectories for the Layzer-type bubble (a) and for the flattened bubble (b). The bubble curvature is ζ_1, the velocity is v, the initial velocity is v_0, and the wave vector is k. The black circle marks the Layzer-type solution; the black square marks the flattened solution.

harmonics, we extended the functional space and took into consideration all bubbles allowed by symmetry of the flow. We found a continuous family of regular asymptotic solutions and studied the solutions' stability. For a fixed value of the spatial period λ, the physically significant solution in the family corresponds to a flattened bubble with radius of curvature $(R/\lambda)\to\infty$, more precisely $R\sim\lambda(t/\tau)^{|\mathrm{Re}[\beta_\infty]|}$, not to a bubble with a finite curvature $R\sim(\lambda/2)$.

A nonuniqueness of regular asymptotic solutions and a separation criterion are well known issues in many free-boundary problems, such as Rayleigh-Taylor [14–19] or Taylor-Saffman [38] instabilities. Using conformal mapping, Garabedian was the first to find in Ref. [12] that singularities result in nonuniqueness of steady solutions for 2D Rayleigh-Taylor bubbles. Our approach provides physical background for Garabedian's reasoning [19] and expands Garabedian's idea to 3D and 2D Richtmyer-Meshkov flows [37]. From the other side, with a particular truncation the dynamical system in Eqs. (2) and (4) can be reduced to the expansion of the Layzer type, if at every N the number of parameters $N_p=0$ and the truncation number $N_t=N_e$ [18,19,29]. The Layzer-type expansion, however, does not capture the interplay of harmonics in the nonlinear dynamics. There is no Layzer-type asymptotic solution, only a first-order approximation. In contrast, within the family of solutions, one can easily find higher-order corrections to the parameters of the Layzer-type bubble, Fig. 1.

Based on the linear analysis in Ref. [29], (2), (4) and on the foregoing results, we expect the following dynamics of the bubble front in the Richtmyer-Meshkov instability. Initially, the bubble is almost flat, $\zeta_1(0)=0$, and its velocity is $v(0)=v_0$. In the linear regime, $t\ll\tau$, the bubble surface becomes curved, $\zeta_1(t)\sim -kt/\tau$, and its velocity decreases, $v(t)-v_0\sim -v_0 t/\tau$. For $t\sim\tau$ the curvature ζ_1 reaches an extreme value dependent on the initial conditions. Asymptotically, $t/\tau\gg 1$, the bubble flattens, $\zeta_1(t)\sim -k(t/\tau)^{-|\mathrm{Re}[\beta_\infty]|}$, and its velocity decay, $v(t)\sim C_\infty/kt$, where constants β_∞ and C_∞ are independent of the initial conditions, Fig. 4. The bubbles in RMI flatten because they decelerate.

Our conclusions agree qualitatively with the existing data: flattening of the nonlinear bubbles has been observed in many experiments and simulations on RMI [8–10,24–28]. Owing to the lack of improved diagnostics, we cannot perform a detailed quantitative comparison with existing data. The bubble displacement is the only diagnostic parameter available in experiments and simulations to date. Our analysis shows that the flattened bubble is significantly faster than the bubble with a finite curvature (approximately four times faster in 3D and three times faster in 2D), Fig. 1. It is hard, however, to pick up this difference from the experimental data. Since in both cases the velocity is $v\sim C/kt$, then, asymptotically the bubble displacement Δh is $\Delta h\sim C\lambda\ln(t/\tau)$. The logarithmic correction is of the order of experimental error, and the coefficient C is indistinguishable. To confirm the validity of our theory, additional diagnostic parameters are required. The flattening of the RM bubble is described by power-law time dependence, therefore, the bubble curvature can be a reliable diagnostic parameter. The main issue that needs to be checked by experiments is the following. Does the curvature of the RM bubble reach with time a finite limiting value (the same as in the RT case) or approach zero? To determine the bubble curvature from the experimental data, one can find a sphere closest to the interface in the vicinity of the bubble top as in Ref. [39]. This kind of data analysis is more efficient than calculations of second-order derivatives of the interface. The flattening exponent $\mathrm{Re}[\beta_\infty]$ can be determined via data presentation in logarithmic scales, $\ln(R/\lambda)$ versus $\ln(t/\tau)$.

As is seen from the foregoing, the 2D and 3D bubbles have similar dynamics. Asymptotically in both 2D and 3D cases the bubble curvature is $\zeta_1(t)\sim -k(t/\tau)^{-|\beta_\infty|}$, the velocity $v(t)\sim C_\infty/kt$, and the displacement $\Delta h\sim C_\infty\lambda\ln(t/\tau)$, with $C_{\infty,3D}/C_{\infty,2D}\approx 2$ and $\mathrm{Re}[\beta_{\infty,3D}]/\mathrm{Re}[\beta_{\infty,2D}]\approx 1$. To distinguish between 2D and 3D dynamics in experiments, a three-dimensional visualization of the flow and measurements of the bubble principal curvatures in the x and y directions are required. At a fixed value of period λ, 3D bubbles are faster than 2D bubbles. This suggests that a 2D coherent structure in RMI would break under modulations into a 3D structure, while the nonlinear 3D bubbles would tend to conserve a near-circular contour [18,19]. A detailed study of the dimensional 3D-2D crossover in RMI will be carried out in the future.

The regular asymptotic solutions in the Richtmyer-Meshkov and Rayleigh-Taylor instability have a number of common properties, Figs. 1–3 [18,19]. In either RT or RM cases there is no Layzer-type asymptotic solution, only a Layzer-type first-order approximation; yet, there is a family of asymptotic solutions, and the number of parameters is determined by the symmetry of the flow [18,19]. However, in contrast to the RM case, the Layzer-type bubble with a finite curvature $R\sim(\lambda/2)$ approximates well the fastest stable solution in the RT family [19]. So, the bubble shape is an important diagnostic parameter, and our theoretical results could serve as a test for experiments and simulations on RTI and RMI.

In most experiments on RMI, fluids have close densities and vorticity influences the mass flux and the pressure distribution in the flow [8–10,24–28]. These effects do not destroy the major qualitative result obtained in the frame of our idealistic theory. The exponent of flattening β_∞ may depend, however, on the density ratio and vorticity. A complete problem has never been studied before and it will be addressed in the future. If fluids have a finite density contrast and the

energy cascade is insignificant then we can apply an analysis similar to the foregoing. For a two-fluid system the regular bubble in RMI flattens asymptotically with time, while the Layzer-type solution breaks the conservation laws and requires mass flux through the interface.

To conclude, we outline the limitations of our theoretical approach. The local analysis is applicable as long as the energy cascade is insignificant, and the spatial period of the 3D or 2D coherent structure in RMI is invariable. The presentation in terms of moments (2), (4) allows one to describe the linear regime of the instability [29], $t \ll \tau$, and to find the multiple harmonic regular asymptotic solution in the highly nonlinear regime, $t \gg \tau$, Fig. 1 and 2. In the intermediate regime of the instability, $t \sim \tau$, singularities develop and produce the cascades of energy. The local analysis neither depicts the dispersive properties of the flow for $t \sim \tau$ nor describes the process of generation of high-order harmonics by singularities. These issues are very important in the field of free-boundary problem [1,13–15] and further theories or computational methods may be able to resolve them.

ACKNOWLEDGMENTS

The work was supported financially by DOE Grant No. DE-FG02-98ER25363 and by the Alexander von Humboldt Foundation. The author is grateful to Dr. J. Glimm, Dr. S. I. Anisimov, Dr. J. Jacobs, Dr. G. Dimonte, Dr. A. Oparin, and Dr. B. Plohr for discussions.

APPENDIX

The expansions of the nonlinear equations in Eq. (1) near the highly symmetric point of the interface (the top of the bubble or spike) have the form

$$\sum_{N=1}^{\infty}\left(\sum_{s,p,q=0}^{s+p+q=N}[(\overline{spq})_t+(\overline{spq})_0]x^{2s}y^{2p}(z^*)^q+\sum_{i=0}^{N}P_i\sum_{s,p,q=0}^{s+p+q=N-l}(\overline{spq})_1x^{2s}y^{2p}(z^*)^q+x\sum_{i=0}^{N}Q_l\sum_{z,p,q=0}^{s+p+q=N-l}(\overline{spq})_2x^{2s}y^{2p}(z^*)^q\right)=0$$

for the momentum equation, and

$$\sum_{N=1}^{\infty}\left(\sum_{s,p,q=0}^{s+p+q=N}[(spq)_t+(spq)_0]x^{2s}y^{2p}(z^*)^q+\sum_{l=0}^{N}P_1\sum_{s,p,q=0}^{s+p+q=N-l}(spq)_1x^{2s}y^{2p}(z^*)^q+\sum_{l=0}^{N}Q_l\sum_{s,p,q=0}^{s+p+q=N-l}(spq)_2x^{2s}y^{2p}(z^*)^q\right)=0$$

for the continuity equation. The coefficients in these expansions have the following form:

$$(\overline{spq})_t=\frac{(-1)^{s+p+q}}{(2s)!(2p)!q!}\dot{M}_{2s,2p,q-1}\quad\text{with}\quad(\overline{000})_1=0,$$

$$(\overline{spq})_0=\frac{1}{2}\frac{(-1)^{s+p+q}}{(2s)!(2p)!q!}\left(-6M_{2s,2p,q}M_{0,0,0}+\sum_{i,j,r=0}^{s,p,q}(3C_{2s}^{2i}C_{2p}^{2j}C_q^pM_{2i,2j,r}M_{2s-2i,2p-2j,q-r}-C_{2s}^{2i+1}C_{2p}^{2j}C_q^rM_{2i+2,2j,p-1}M_{2s-2i,2p-2j,q-r-1}-C_{2s}^{2i}C_{2p}^{2j+1}C_q^rM_{2i,2j+2,r-1}M_{2s-2i,2p-2j,q-r-1})\right)$$

with $(\overline{000})_0=(\overline{001})_0=0$,

$$(\overline{sqp})_1=-\frac{(-1)^{s+p+q}}{(2s+1)!(2p)!q!}\left(-M_{2s+2,2p,q-1}M_{0,0,0}+\sum_{i,j,r=0}^{s,p,q}C_{2s}^{2i+1}C_{2p}^{2j}C_q^rM_{2i+2,2j,r-1}M_{2s-2i,2p-2j,q-r}\right),$$

$$(\overline{sqp})_2=-\frac{(-1)^{s+p+q}}{(2s)!(2p+1)!q!}\left(-M_{2s,2p+2,q-1}M_{0,0,0}+\sum_{i,j,r=0}^{s,p,q}C_{2s}^{2i}C_{2p}^{2j+1}C_q^rM_{2i,2j+2,r-1}M_{2s-2i,2p-2j,q-r}\right)$$

with $(\overline{000})_1=(\overline{000})_2=0$,

$$(sp0)_t=\dot{\zeta}_{sp}\quad\text{with}\quad(spq)_t=0\quad\text{for all}\quad q\neq 0;$$

$$(sqp)_0=\frac{(-1)^{s+p+q}}{(2s+1)!(2p)!q!}\left(-2M_{2s+2,2p,q-1}M_{0,0,0}+\sum_{i,j,r=0}^{s,p,q}C_{2s}^{2j}C_{2p}^{2j}C_q^r M_{2i,2j,r-1}M_{2s-2i,2p-2j,q-r}\right),$$

$$(sqp)_1=-\frac{(-1)^{s+p+q}}{(2s+1)!(2p)!q!}M_{2s+2,2p,q-1}\quad\text{with}\quad(sqp)_2=-\frac{(-1)^{s+p+q}}{(2s)l(2p+1)lq!}M_{2s,2p+2,q-1}$$

with $(000)_0=0$, $(000)_1=-M_{2,0,-1}$ and $(000)_2=-M_{0,2,-1}$;

$$P_1=\sum_{l=0}^{l}2i\zeta_{i,l-i}x^{2i}y^{(l-i)},\quad Q_l=\sum_{i=0}^{l}2(l-i)\zeta_{i,l-i}x^{2i}y^{2(l-i)}\quad\text{with}\quad P_0=Q_0=0,$$

$$z^*=\sum_{l=0}^{\infty}\sum_{l=0}^{l}\zeta_{i,l-i}x^{2i}y^{2(l-i)}\quad\text{with}\quad\zeta_{00}=0.$$

In the above expressions, dot marks time derivative, $C_q^r=q!/r!(q-r)!$, N is the order of approximation, and N, s, p, q, i, j, r, l, are integers. In the case of square symmetry $M_{a,b,c}=M_{b,a,c}$ and $M_{a+2,b,c-1}+M_{a,b+2,c-1}=M_{a,b,c+1}$.

For a flow in a gravity field, the term $g(t)z|_{z=z}$ is added on the left-hand side of the momentum equation in Eq. (1), and the coefficient $(\overline{001})_0=g(t)$. The case of $g(t)=g>0$ corresponds to the Rayleigh-Taylor instability.

[1] H. J. Kull, Phys. Rep. **206**, 197 (1991); V. Rupert, in *Shock Waves*, Proceedings of the 18th International Symposium on Shock Waves, edited by K. Takayama (Springer-Verlag, Berlin, 1992).

[2] R. M. Davies and G. I. Taylor, Proc. R. Soc. London, Ser. A **200**, 375 (1950).

[3] R. D. Richtmyer, Commun. Pure Appl. Math. **13**, 297 (1960); E. E. Meshkov, Sov. Fluid. Dyn. **4**, 101 (1969).

[4] K. I. Read, Physica D **12**, 45 (1984).

[5] M. M. Marinak *et al.*, Phys. Rev. Lett. **80**, 4426 (1998).

[6] G. Dimonte and M. Schneider, Phys. Fluids **12**, 304 (2000).

[7] M. Schneider, G. Dimonte, and B. Remington, Phys. Rev. Lett. **80**, 3507 (1998).

[8] N. N. Anuchina, Yu. A. Kucherenko, V. E. Neuvazhaev, V. N. Ogibina, I. I. Shibarshov, and V. G. Yakovlev, Izv. Akad. Nauk SSSR, Mekh. Zhidk. Gaza **6**, 157 (1978).

[9] A. N. Aleshin, E. V. Lazareva, S. G. Zaytsev, V. B. Rozanov, E. G. Gamalii, and I. G. Lebo, Sov. Phys. Dokl. **35**, 159 (1990).

[10] J. W. Jacobs and J. M. Sheeley, Phys. Fluids **8**, 405 (1996).

[11] D. Layzer, Astrophys. J. **122**, 1 (1955).

[12] P. R. Garabedian, Proc. R. Soc. London, Ser. A **241**, 423 (1957).

[13] G. R. Baker, D. I. Meiron, and S. A. Orszag, J. Fluid Mech. **123**, 477 (1982); Phys. Fluids **23**, 1485 (1980).

[14] S. Tanveer, Proc. R. Soc. London, Ser. A **441**, 501 (1993).

[15] J. A. Zuffiria, Phys. Fluids **31**, 3199 (1988).

[16] N. A. Inogamov, Sov. Phys. JETP **55**, 521 (1992).

[17] G. Hazak, Phys. Rev. Lett. **76**, 4167 (1996).

[18] S. I. Abarzhi, Phys. Rev. E **59**, 1729 (1999); Sov. Phys. JETP **83**, 1012 (1996); Phys. Fluids **13**, 2182 (2001).

[19] S. I. Abarzhi, Phys. Rev. Lett. **89**, 1332 (1998).

[20] S. W. Haan, Phys. Fluids B **3**, 2349 (1991); J. G. Wouchuk and K. Nishihara, Phys. Plasmas **3**, 376 (1996).

[21] A. L. Velikovich and G. Dimonte, Phys. Rev. Lett. **76**, 3112 (1996).

[22] Q. Zhang and S. Sohn, Phys. Lett. A **212**, 149 (1996).

[23] X. L. Li and Q. Zhang, Phys. Fluids **9**, 3069 (1997).

[24] R. L. Holmes *et al.*, J. Fluid Mech. **389**, 55 (1999).

[25] R. Holmes, J. W. Grove, and D. H. Sharp, J. Fluid Mech. **301**, 51 (1995).

[26] J. Grove, Adv. Appl. Math. **10**, 201 (1989).

[27] Volkov *et al.*, Tech. Phys. Lett. **27**, 20 (2001).

[28] A. D. Kotel'nikov, J. Ray, and N. Zabusky, Phys. Fluids **12**, 3245 (2000).

[29] S. Abarzhi, Phys. Fluids **11**, 1015 (2000).

[30] K. O. Mikaelian, Phys. Rev. E **47**, 375 (1993); Phys. Rev. A **42**, 7211 (1990).

[31] These are hexagonal $p6mm$, square $p4mm$, rectangular $p2mm$, rhombic cmm, and oblique $p2$ symmetry groups. For international classification of two-dimensional crystallographic groups the reader can see the book A. V. Shubnikov and V. A. Koptsik, *Symmetry in Science and Art* (Plenum Press, New York, 1979).

[32] J. Hecht, U. Alon, and D. Shvarts, Phys. Fluids **6**, 4019 (1994).

[33] N. A. Inogamov, Sov. Phys. JETP **80**, 890 (1995).

[34] K. O. Mikaelian, Phys. Rev. Lett. **80**, 508 (1998).

[35] Q. Zhang, Phys. Rev. Lett. **81**, 3391 (1998).

[36] For oblique symmetry and rhombic symmetry $N_p=3$ (two principal curvatures and their position with respect to axes); for rectangular symmetry $N_p=2$ (two principal curvatures); for square symmetry and hexagonal symmetry as well as for a 2D case $N_p=1$ (single principal curvature).

[37] S. I. Abarzhi, Phys. Lett. A **294**, 95 (2002).

[38] P. G. Saffman and G. I. Taylor, Proc. R. Soc. London, Ser. A **245**, 312 (1958); S. Tanveer, Phys. Fluids **30**, 1589 (1987); G. L. Vasconcelos and L. P. Kadanoff, Phys. Rev. A **44**, 6490 (1991).

[39] A. Oparin and S. Abarzhi, Phys. Fluids **11**, 3306 (1999).